International Journal of Nanomedicine

Dovepress
open access to scientific and medical research

Open Access Full Text Article

ORIGINAL RESEARCH

Multifunctional Immunoliposomes Combining Catalase and PD-L1 Antibodies Overcome Tumor Hypoxia and Enhance Immunotherapeutic Effects Against Melanoma

This article was published in the following Dove Press journal:
International Journal of Nanomedicine

Yu Hei[1]
Binhong Teng[2,3]
Ziqian Zeng[2,3]
Siqi Zhang[3]
Qian Li[3]
Jijia Pan[3]
Zuyuan Luo[3]
Chunyang Xiong[1]
Shicheng Wei[2,3]

[1]Department of Mechanics and Engineering Science, College of Engineering, Peking University, Beijing, People's Republic of China; [2]Department of Oral and Maxillofacial Surgery, School and Hospital of Stomatology, Peking University, Beijing, People's Republic of China; [3]Laboratory of Biomaterials and Regenerative Medicine, Academy for Advanced Interdisciplinary Studies, Peking University, Beijing, People's Republic of China

Correspondence: Chunyang Xiong
Department of Mechanics and Engineering Science, College of Engineering, Peking University, Beijing, People's Republic of China
Tel +86 10 62757940
Email cyxiong@pku.edu.cn

Shicheng Wei
Department of Oral and Maxillofacial Surgery, School and Hospital of Stomatology, Peking University, Beijing, People's Republic of China
Tel +86 10 82195780
Email sc-wei@pku.edu.cn

Background: Immune checkpoint blockades (ICBs) are a promising treatment for cancers such as melanoma by blocking important inhibitory pathways that enable tumor cells to evade immune attack. Programmed death ligand 1 monoclonal antibodies (aPDL1s) can be used as an ICB to significantly enhance the effectiveness of tumor immunotherapy by blocking the PD-1/PD-L1 inhibitory pathway. However, the effectiveness of aPDL1s may be limited by low selectivity in vivo and immunosuppressed tumor microenvironment including hypoxia.

Purpose: To overcome the limitations, we develop a multifunctional immunoliposome, called CAT@aPDL1-SSL, with catalase (CAT) encapsulated inside to overcome tumor hypoxia and aPDL1s modified on the surface to enhance immunotherapeutic effects against melanoma.

Methods: The multifunctional immunoliposomes (CAT@aPDL1-SSLs) are prepared using the film dispersion/post-insertion method. The efficacy of CAT@aPDL1-SSLs is verified by multiple experiments in vivo and in vitro.

Results: The results of this study suggest that the multifunctional immunoliposomes preserve and protect the enzyme activity of CAT and ameliorate tumor hypoxia. Moreover, the enhanced cellular uptake of CAT@aPDL1-SSLs in vitro and their in vivo biodistribution suggest that CAT@aPDL1-SSLs have great targeting ability,resulting in improved delivery and accumulation of immunoliposomes in tumor tissue.Finally, by activating and increasing the infiltration of $CD8^+$ T cells at the tumor site, CAT@aPDL1-SSLs inhibit the growth of tumor and prolong survival time of mice,with low systemic toxicity.

Conclusion: In conclusion, the multifunctional immunoliposomes developed and proposed in this study are a promising candidate for melanoma immunotherapy, and could potentially be combined with other cancer therapies like radiotherapy and chemotherapy to produce positive outcomes.

Keywords: immunotherapy, programmed death ligand 1 monoclonal antibodies, aPDL1s, tumor hypoxia, melanoma, liposomes

Introduction

Tumors can evade and suppress the immune system by multiple mechanisms that hinder the effectiveness of cancer immunotherapy. Two simultaneously performed strategies for overcoming these limiting mechanisms are blocking inhibitory pathways and disrupting the immunosuppressed microenvironment. An immune

checkpoint pathway exploiting the natural T cell suppressive efficacy of the immune checkpoint protein is one example of such an inhibitory mechanism.[1] Inhibitory receptors are commonly overexpressed on the surfaces of tumor cells. Overexpression is the product of inflammation and antigen stimulation, which makes inhibitory receptors logical targets for monoclonal antibody (mAb) inhibition.[2,3] Compare to other solid tumor types, melanoma which frequently displays tumor-infiltrating lymphocytes and regression on histology may express higher level of inhibitory receptors.[4] The mAbs which can specifically bind to inhibitory receptors such as legend of the programmed cell death protein 1(aPDL1) can inhibit melanoma growth efficiently. Over the last five years, the United States Food and Drug Administration (FDA) has approved some aPDL1 biologics (such as pembrolizumab and nivolumab) for the treatment of melanoma.[5] These aPDL1 biologics effectively inhibit the growth of melanoma and prolong the survival time of patients. Despite notable advances, autoimmune disorders and inflammatory side effects from aPDL1s continue to hinder the effectiveness of ICBs for melanoma treatment.[6–9] Side effects are thought to be caused by non-specific T cell-mediated responses, whereby reactivity is directed against normal cells. These responses are associated with the low selectivity of aPDL1s.[10,11] Accordingly, the delivery of aPDL1s must be improved to allow for selective distribution at the tumor site and increase the effectiveness of immunotherapy while reducing side effects for patients.

Overcoming hypoxia and remodeling the tumor microenvironment could also increase sensitivity to PD-L1 blockades, enhance intratumoral T cell function, and promote tumor regression.[12] Tumors produce a suppressive microenvironment that inhibits T cell activation and promotes T cell apoptosis, which are caused by the recruitment of suppressive regulatory T cells and the secretion of suppressive cytokines.[13] Hypoxia is an important component of the tumor suppressive microenvironment that negatively impacts the activation of T cells by producing an accumulation of cyclic adenosine monophosphate (cAMP) and inhibiting the T cell receptor (TCR) signaling pathway.[14–16] To overcome hypoxia, the antioxidant enzyme catalase (CAT) (Sigma Aldrich,St. Louis, USA) may decompose hydrogen peroxide (H_2O_2) in tumor cells into H_2O and O_2,leading to the reduction of hypoxia-inducible factor (HIF)-1α[17] and enhancing the effectiveness of immunotherapy.[18] In short, we suggest that combining aPDL1s and CAT in a liposome delivery system may be an effective strategy for enhancing the effects of aPDL1s and inhibiting tumor growth.

Liposomes are effective drug delivery vehicles for biological and practical reasons. They can deliver active biological substances, enhance the stability of drugs, reduce systemic toxicities, and enhance drug distribution selectivity.[19–22] Designing liposomes that actively target the site of action is also a practical strategy for improving the selectivity of a drug in vivo, reducing systemic toxicities, and enhancing a drug's therapeutic effects, considering that liposomes are effective nanocarriers.[20,23]

Here, we prepared multifunctional immunoliposomes (termed CAT@aPDL1-SSLs; Figure 1) that effectively target melanoma because of the aPDL1s on the surface and internally encapsulated CAT that significantly reduces hypoxia. CAT encapsulated in liposomes retains its enzymatic activity and is protected against protease hydrolysis. aPDL1 can become inserted into the lipid bilayers of liposomes by reacting with DSPE-Hyd-PEG2000-NHS, which contains a hydrazone bond (a pH-sensitive bond), to form the lead compound DSPE-Hyd-PEG2000-aPDL1 (DSPE:1,2- distearoyl-sn-glycero-3-phosphoethanolamine (PEG: polyethyleneglycol; Hyd: hydrazone)). The liposomes exhibit pH-sensitive characteristics due to the hydrazone bond on the surface. In the acidic tumor microenvironment (pH 6.5), the hydrazone bond reacts with hydrogen ions (H^+) to reduce acidity; aPDL1 is then released and binds to the PD-L1 receptor on tumor cells to block the PD-1/PD-L1 pathway. When many hydrogen ions are consumed, the hydrazone bond will no longer be cleaved, and the entire CAT@aPDL1-SSL structure will bind to the PD-L1 receptor because of the aPDL1s on the surface (Figure 1). Thus, CAT@aPDL1-SSL exhibits excellent targeting ability; the material can be delivered to and accumulate in tumor tissue as demonstrated by cellular uptake in vitro and biodistribution in vivo. The immunoliposomes inhibit tumor growth and prolong the survival of mice by activating, and increasing the infiltration of, $CD8^+$ T cells, with low systemic toxicity. All outcomes indicate that immunoliposomes containing both CAT and aPDL1 have a bright future in terms of melanoma immunotherapy.

Materials and Methods

Materials

1. (2′-Benzothiazolyl)-7-diethylaminocoumarin (Cou-6) was purchased from Aladdin Bio-Chem

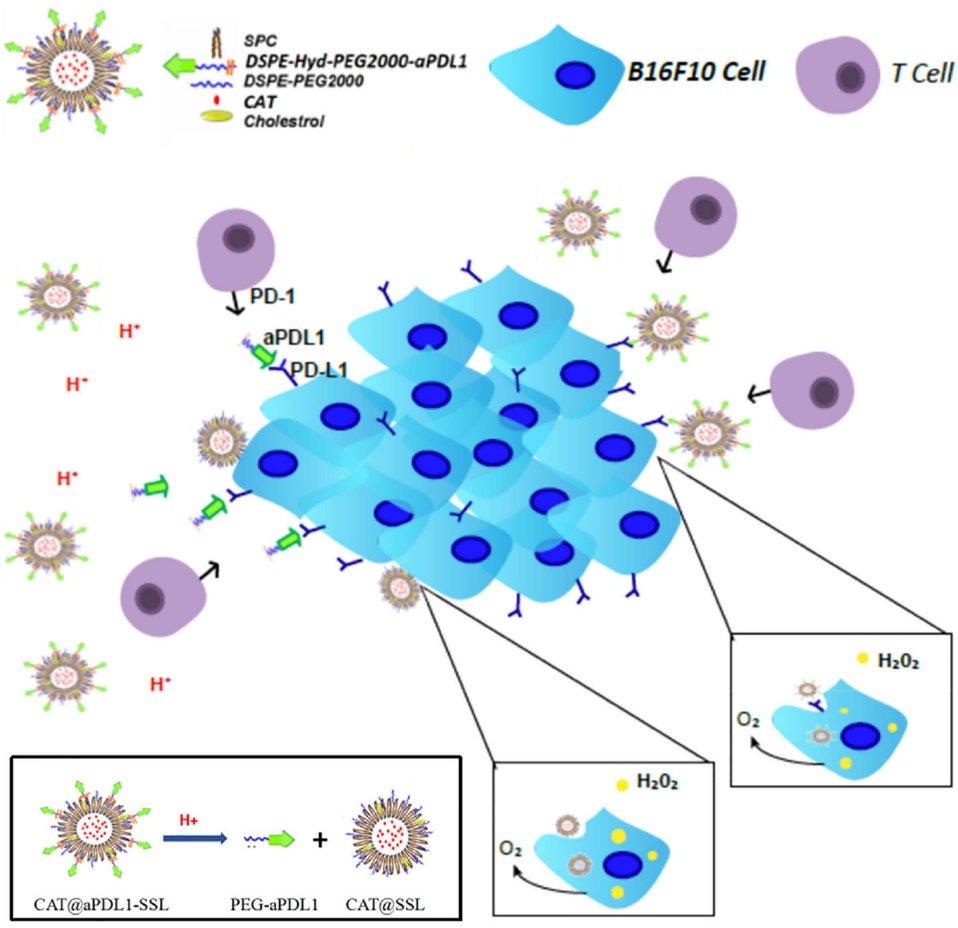

Figure 1 The schematic diagram of the structure and activating mechanism of CAT@aPDL1-SSL.
Note: CAT@aPDL1-SSLs block the PD-1/PD-L1 pathway and deliver CAT into tumor cells to relieve hypoxia, promoting T lymphocyte infiltration and enhancing immunotherapeutic effects.
Abbreviations: aPDL1, programmed death ligand 1 monoclonal antibody; CAT, catalase; SSL, sterically stabilized liposome; aPDL1-SSLs, aPDL1 modified immunoliposomes; CAT@aPDL1-SSLs, CAT-loaded and aPDL1 modified immunoliposomes; SPC, Lecithin (soy beans); DSPE-PEG2000, Distearoylphosphatidylethanoloamine-methoxy-polyethylene glycol MW:2000; Hyd, hydrazine; PD-1, programmed death receptor 1; PD-L1, programmed death ligand 1.

Technology Co. Ltd. (Shanghai, China). Calatase (CAT, 35,000 units/mg protein) and cholesterol were purchased from Sigma Aldrich (St. Louis, USA). Distearoylphosphatidylethanoloamine-methoxy-polyethylene glycol MW:2000 (DSPE-PEG2000) and 1,2-distearoyl-sn-glycero-3-phosphoethanolamine-N- [succinimidyl (polyethylene glycol)] (DSPE-PEG2000-NHS) were purchased from Corden Pharma (Eichenweg, Switzerland). DSPE-hydrazone (Hyd)-PEG2000-NHS was purchased from Xi'an Ruixi Biological Technology Co. Ltd. (Xi'an, China).

Cell Lines and Animals

The mouse melanoma cell line,B16F10,was purchased from Cell Resource Center, Institute of Basic Medical Sciences, Chinese Academy of Medical Sciences.The B16F10 cells were maintained in Dulbecco's modified eagle medium (DMEM) (Gibco, Invitrogen, USA) supplemented with 10% fetal bovine serum (Gibco, Invitrogen, USA),100 U mL−1 penicillin (Invitrogen), and 100 U mL−1 streptomycin (Invitrogen). C57BL/6 mice were purchased from Beijing Vital River Laboratory Animal Technology Co., Ltd. (Beijing, China). Age-matched (6–8 weeks) female animals were used throughout all animal experiments. All animal experiments were conducted following the animal protocols approved by the Ethics Committee on Laboratory Animal Welfare of Peking University.

Preparation of Liposomes

Basic sterically stabilized liposomes (SSLs) were prepared using the film dispersion method.[24] SSLs containing SPC (Lecithin (soy beans)) (Corden Pharma,Eichienweg, Switzerland), cholesterol, and DSPE-PEG2000 were

dissolved in 1 mL of chloroform at a molar ratio of 100:50:8. They were then dried under vacuum to remove residual chloroform and obtain a thin lipid film. The thin lipid films were dispersed in 2 mL of phosphate-buffered saline (PBS) for hydration. The final SSLs were prepared after filtration through two 200 nm polycarbonate membrane filters (Millipore, Billerica, USA).

The multifunctional immunoliposomes (CAT@aPDL1-SSLs) were prepared using the film dispersion/post-insertion method. First, DSPE-Hyd-PEG2000-NHS and a coupling lipid were mixed with aPDL1(Clone:10F.9G2) (Bio X Cell, West Lebanon, NH, USA) at a molar ratio of 10:1 to form the leading compound, DSPE-Hyd-PEG2000-aPDL1, via ester conjugation between the antibody amine group and DSPE-Hyd-PEG2000-NHS.[25] The leading compound DSPE-Hyd-PEG2000-aPDL1 was identified by X-ray photoelectron spectroscopy (XPS; AXIS His-165 Ultra; Kratos Analytical, Shimadzu Corporation, Japan).[26] To reduce costs, we synthesized DSPE-PEG2000-aPDL1 without a hydrazone bond to detect using XPS. To prepare CAT@SSL, the dried lipid was hydrated using 2 mL PBS containing 3 mg CAT. DSPE-Hyd-PEG2000-aPDL1 was then incubated with CAT@SSL at a ratio of 1:100 for 4 h with continuous stirring to form CAT@aPDL1-SSLs. Excessive aPDL1 and CAT were removed using a dialysis membrane with a 300-kDa molecular weight cutoff (MWCO) (Mmbio, China).[23] Coumarin-6 (Cou-6)-loaded liposomes (C6@aPDL1-SSLs) and DiR (1,1-dioctadecyl-3,3,3,3-tetramethylindotricarbocyanine)-loaded liposomes (DiR@aPDL1-SSLs) were also prepared using the film dispersion method.

Liposome Characterization

Particles Size, Morphology and Catalytic Activity

The particle size and polydispersity of CAT@aPDL1-SSL multifunctional immunoliposomes were measured using dynamic light scattering (DLS) (Zetasizer Nano ZS90; Malvern, United Kingdom). Transmission electron microscopy (TEM) (JEM-1400Plus; JEOL, Tokyo, Japan) was used to observe the morphology of CAT@aPDL1-SSLs after the sample was stained with 2% (w/v) phosphotungstic acid solution. The encapsulation efficiency (EE) of CAT was measured using the standard bicinchoninic acid (BCA) protein assay (Solarbio Science & Technology Co., Ltd, Beijing, China). EE% was calculated using Equation (1).

$$EE(\%) = \frac{\text{Weight of the CAT in liposomes}}{\text{Weight of the feeding CAT}} \times 100\% \quad (1)$$

The catalytic activities of free CAT and CAT encapsulated in liposomes were determined using the standard Goth's method.[27,28] First, 0.5 mL of H_2O_2 solution (30% water solution) was added to 1.5 mL Eppendorf (EP) tubes, then 1 mL of free CAT and 1 mL of CAT@aPDL1-SSLs were added to each EP tube and reacted with H_2O_2 at 37°C for 1 min. Subsequently, 0.5 mL of ammonium molybdate (32.4 mM) was added to the reaction solution. The reaction was stopped once the ammonium molybdate reacted with excessive H_2O_2 solution to produce stable yellow primrose complexes. The yellow primrose complexes were detected using a UV–vis spectrometer (Lambda 35; PerkinElmer, Waltham, MA, USA) at a wavelength of 400 nm. The relative catalytic activity was calculated using Equation (2).

$$\text{Relative catalytic activity}(\%) = \frac{(A_{PBS} - A_{x(t)})}{(A_{PBS} - A_{x(0)})} \times 100\% \quad (2)$$

where A_{PBS} is the absorbance of H_2O_2 with PBS; $A_{x(t)}$ the absorbance of H_2O_2 after exposure to CAT or CAT@aPDL1-SSL for t h; and $A_{x(0)}$ the absorbance of H_2O_2 after exposure to CAT or CAT@aPDL1-SSL for 0 h.

The stability of CAT or CAT@aPDL1-SSLs against protease was also detected. CAT and CAT@aPDL1-SSLs were mixed with protease K and the catalytic activity was detected by Goth's method as noted above. A portable dissolved oxygen meter (JPBJ-608; INESA, Shanghai, China) was used to detect the catalytic activity of CAT@aPDL1-SSLs by detecting the dissolved oxygen concentration in H_2O_2 solution at different times.

The Presence of aPDL1s on the Surface of Liposomes

C6@aPDL1-SSLs and Alexa Fluor 647-labelled goat anti-rabbit immunoglobulin secondary antibody (Abcam, Cambridge, USA) were used to confirm that aPDL1s were successfully attached to the surface of the liposomes. C6@aPDL1-SSLs (pH 7.4) were incubated with the secondary antibodies for 2 h at room temperature. After incubation, the mixtures were centrifuged at 14,000 rpm for 15 min and washed twice using PBS. The sediment was then resuspended in PBS and observed using confocal laser scanning microscopy (CLSM) (A1Rsi; Nikon, Tokyo, Japan). To investigate the activity of aPDL1 on the surface of liposomes at low pH conditions, the solution

was adjusted to pH 6.5 using citrate buffer (pH 6.0) and the subsequent steps were repeated as described above.

Cellular Uptake of Liposomes in vitro

C6-loaded liposomes were prepared using the film dispersion method noted above. B16-F10 cells were seeded into six-well plates at a density of 1×10^6 cells/well and incubated overnight. The culture media was then removed and the cells were washed three times using PBS. PBS, free C6, C6@aPDL1-SSLs, C6@aPDL1-SSLs, and free aPDL1 (pH 7.4) were added into each well of the plates (C6, 150 ng/mL; aPDL1, 0.01mg/mL) and incubated with B16-F10 cells for 2 h at 37°C in the presence of 5% CO_2. After 2 h, samples were removed and 200 μL trypsin with ethylene diamine tetraacetic acid (EDTA) was added into each well to detach the cells. Suspended cells were centrifuged at 1,000 rpm for 5 min and the sediment was resuspended in PBS at a density of 1×10^6 cells/mL. To investigate the cellular uptake of liposomes in low pH conditions, the culture medium was adjusted to pH 6.5 using citrate buffer (pH 6.0) and the subsequent steps were repeated as described above. Flow cytometry (FACS Calibur; BD Biosciences, San Jose, CA, USA) was used to detect the cellular uptake of liposomes. Flow cytometry results were processed using Flow Jo 10.0 software.

Biodistribution of Liposomes in vivo

To study the biodistribution and targeting ability of multifunctional immunoliposomes in vivo, DiR, a lipophilic fluorescent probe, was used to label the liposomes. DiR-loaded liposomes were prepared using the film dispersion method noted above. C57BL/6 (6–8 weeks of age, 20 g/b) mice were injected with B16-F10 cells subcutaneously in the right flank at a density of 1×10^6. When the tumor volume reached 100 mm^3, the tumor-bearing mice were divided into three randomized groups. They were then intravenously injected with free DiR, DiR@SSLs, or DiR@aPDL1-SSLs (DiR: 150 μg/kg). The biodistribution of the liposomes was observed using an in vivo optical imaging system (IVIS Spectrum, Xenogen, Alameda, CA, USA) at 1, 2, 4, 8, 12, and 24 h post-liposome injection. Mice were sacrificed after 24 h and the tumors and main organs were harvested for imaging in vitro. The images were processed using Living Image 4.3.1 software.

Evaluation of the Tumor Hypoxia Evolution

To evaluate the ability of liposomes to relieve tumor hypoxia, tumor-bearing C57BL/6 mice were intravenously injected with PBS, aPDL1-SSLs, CAT@SSLs, or CAT@aPDL1-SSLs (CAT: 2 mg/kg; aPDL1: 1 mg/kg). At 24 h after intravenous injection, pimonidazole hydrochloride (60 g/20 g) was intraperitoneally injected into each mouse (Hypoxyprobe-1 Plus kit; Hypoxyprobe, Inc., Burlington, MA, USA).[27] The mice were then sacrificed and the tumors were harvested for immunofluorescence staining. For detection of hypoxia-inducible factor (HIF)-1α,tumor sections were incubated with mouse anti-HIF-1α antibody (CST, Danvers, MA,USA) and Alexa Fluor 647-labelled goat anti-rabbit immunoglobulin secondary antibody (Abcam, Cambridge, USA) following the instructions of the Manufacturers.Cell nuclei were stained with 4′,6-diamidino-2-phenylindole (DAPI) (Solarbio, China).The results of immunofluorescence staining were observed using CLSM (Nikon,A1R-si,Japan). Semi-quantitative results of tumor hypoxia regions were analyzed using Image J software. The positive hypoxia area was calculated using Equation (3).

$$\text{The hypoxia positive area}(\%) = \frac{\text{the area of fluorescence of hypoxia maker}}{\text{total area}} \times 100\% \quad (3)$$

Infiltration of T Lymphocytes in Tumor Tissue

To evaluate the infiltration of T lymphocytes in tumor tissue, tumor-bearing C57BL/6 mice were prepared using the method described above. When the tumor volume reached 100 mm^3, the tumor-bearing mice were divided into five groups and randomly intravenously injected with PBS, free aPDL1SSLs, aPDL1-SSLs, or CAT@aPDL1-SSLs (aPDL1: 1 mg/kg). At 24 h after intravenous injection, the mice were sacrificed and the tumors were harvested for immunofluorescence staining. 4′,6-diamidino-2-phenylindole (DAPI) (Solarbio, China) was used to label the nuclei of B16-F10 cells, and $CD4^+$ and $CD8^+$ antibodies (Bioss, Shanghai, China) were used to label the T lymphocytes in tumor tissue.The results of immunofluorescence staining were observed using CLSM (Nikon,A1R-si,Japan).The infiltration of T lymphocytes in tumor tissue was further assessed by fluorescence activated cell sorting (FACS) (FACS Calibur; BD Biosciences,San Jose,CA,USA).Tumors were harvested and digested by hyaluronidase/collagenase IV and DNase I with the shaker for an hour at 37°C to obtain the single cell suspension.The cells were filtered through 40 μm filters after washed three times and the red blood cells were removed by using red blood cell lysis buffer (Solarbio, China). Then the T lymphocytes were incubated with

phycoerythrin (PE)-labelled mouse anti-CD3 antibody,Alexa Fluor 488-labelled anti-CD4 antibody and Alexa Fluor 647-labelled anti-CD8 antibody (Bioss, Shanghai, China) after the Fc block of the cells.

Antitumor Efficacy and Safety Study in vivo

To evaluate the antitumor efficacy of the liposomes, the tumor-bearing mice were randomly divided into six groups (n = 6) and intravenously injected with PBS, free aPDL1, SSLs, aPDL1-SSLs, CAT@SSLs, or CAT@aPDL1-SSLs (aPDL1: 1 mg/kg) every 3 days. During the treatment period, the weight of the mice and the volume of their tumors were recorded to evaluate the antitumor efficacy of each treatment. The tumor volumes were calculated by the formulation: $V = \text{length} \times \text{width}^2/2$. The survival curve of tumor-bearing mice was analyzed using GraphPad Prism 7.0 software. Finally, to evaluate the safety of using liposomes in vivo, the main organs of mice were collected for hematoxylin and eosin (H&E) staining.

Statistical Analysis

The data are presented as the means ± SD. Mean value were compared using the two-tailed Student's *t*-test. $P < 0.05$(*), $P < 0.01$(**), and $P < 0.001$(***) were considered statistically significant.

Results and Discussion

Characterization of Immunoliposomes

Particles Size, Morphology and Catalytic Activity

Multifunctional immunoliposomes were prepared using the film dispersion/post-insertion method. The structure and activating mechanism of the CAT@aPDL1-SSLs were shown in Figure 1. DSPE-Hyd-PEG2000-aPDL1, the leading compound inserted into the lipid bilayer of the liposomes, was detected by XPS. Changes in nitrogen signals relating to specific binding energies demonstrated that DSPE-Hyd-PEG2000-NHS was successfully conjugated with aPDL1 following the reaction of N-hydroxysuccinimide (NHS) and an amine of aPDL1.[25] To reduce costs, materials without hydrazone bonds were used as substitutes for reaction and detection. There was no distinct signal peak from the orbital of nitrogen (N 1s), as shown in Figure S1A, demonstrating that DSPE-PEG2000 and aPDL1 did not form the ester conjugation. However, the distinct peak of N1s signal from DSPE-PEG2000-NHS and aPDL1 confirmed that aPDL1 successfully conjugated with DSPE-PEG2000-NHS to form the compound DSPE-PEG2000-aPDL1 (Figure S1B). The conjugation between aPDL1 and DSPE-PEG2000-NHS was likely an ester conjugation between an amine of aPDL1 and the NHS of DSPE-PEG2000-NHS.[25] In short, these findings (Figure S1) indicated that aPDL1 could successfully conjugate with DSPE-Hyd-PEG2000-NHS to form the leading compound DSPE-Hyd-PEG2000-aPDL1 via an ester conjugation between the amine of aPDL1 and the NHS of DSPE-Hyd-PEG2000-NHS.

The particle size of CAT@aPDL1-SSL was 118.2 ± 1.763 nm, and its polydispersity was 0.223 ± 0.007, determined by dynamic light scattering (DLS) (Figure 2A). The small particle size of CAT@aPDL1-SSLs may enhance their accumulation in tumor tissue via the enhanced permeability and retention (EPR) effect.[29] CAT@aPDL1-SSLs had a spherical structure and good dispersion capabilities according to TEM observations (Figure 2B).

The encapsulation efficiency (EE) of CAT was determined to be 36% using the standard bicinchoninic acid (BCA) protein assay.The catalytic ability of CAT encapsulated in liposomes was determined using the Goth method and a portable dissolved oxygen meter. CAT@aPDL1-SSLs increased the O_2 concentration in H_2O_2 solution from 4.41 mg/mL to 31.08 mg/mL, whereas SSLs did not exhibit any significant influence on O_2 concentration in H_2O_2 solution compared to that of PBS. This suggests that CAT encapsulated in liposomes had the ability to decompose H_2O_2 to produce O_2 (Figure 2C). Because proteases were present in vivo, the influence of proteases on free CAT and CAT@aPDL1-SSLs were detected to determine whether liposomes could protect the catalytic ability of CAT. CAT@aPDL1-SSLs retained 80.76% of the original catalytic ability after treatment with protease K (0.5 mg/mL) at 37°C for 8 h (Figures 2D and S2A, B) using a protease K digestion assay.[27,30,31] However, free CAT only maintained 32.41% of its catalytic ability after protease K digestion (Figures 2D and S2A, B). The protease K digestion assay suggested that the liposomes not only deliver CAT but also protect the catalytic ability of CAT encapsulated inside the liposomes, and prevent CAT from being digested by proteases.

The Presence of aPDL1s on the Surface of Liposomes

To confirm the presence of aPDL1s on the surface of liposomes, a liposome- encapsulated C6 (Coumarin-6) lipophilic green fluorescent probe was prepared using the film dispersion method. Alexa Fluor 647-labelled secondary antibody was used to label aPDL1 on the surface of

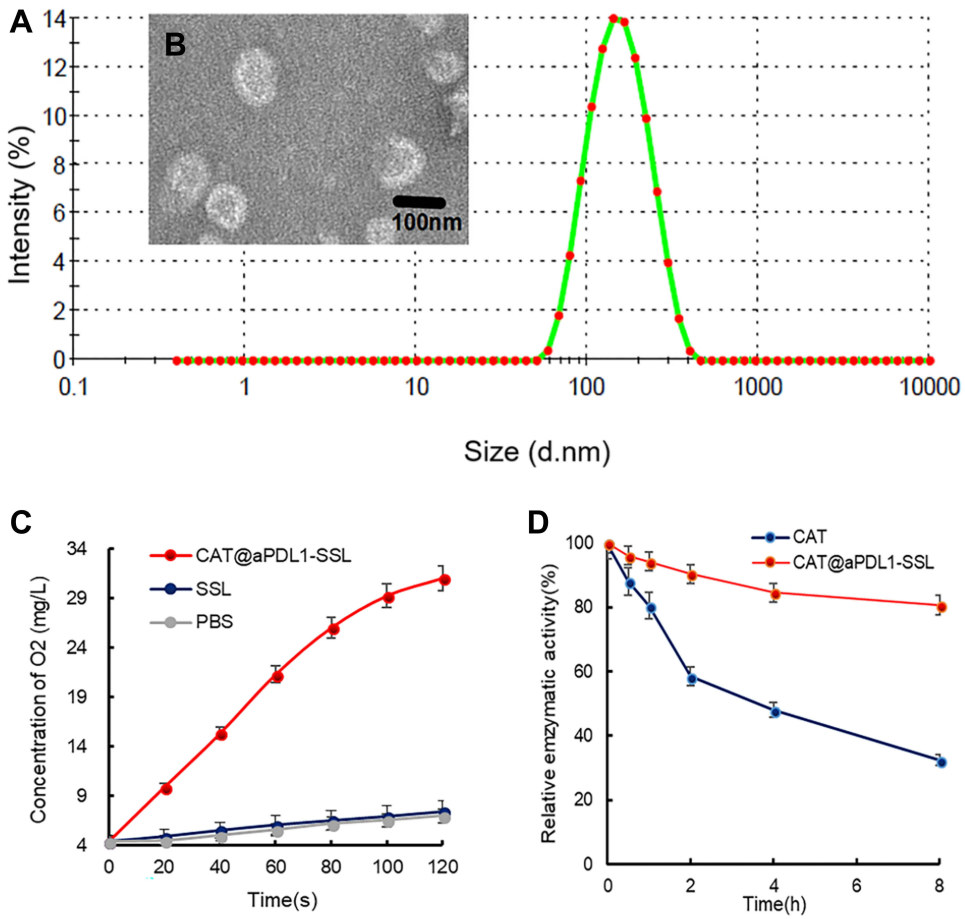

Figure 2 Characterization of CAT@aPDL1-SSLs.
Notes: (**A**) The particle size distribution of CAT@aPDL1-SSLs determined by DLS. (**B**) Morphological images observed by TEM. Scale bar: 100 nm. (**C**) Concentrations of O_2 in H_2O_2 solution detected by a portable dissolved oxygen meter after adding CAT@aPDL1-SSLs and SSLs. (**D**) Relative catalytic ability of free CAT and CAT@aPDL1-SSLs at different time points after protease K treatment (0.5 mg/mL).
Abbreviations: CAT, catalase; CAT@aPDL1-SSLs,CAT-loaded immunoliposomes; DLS, dynamic light scattering; TEM, transmission electron microscopy.

C6@aPDL1-SSLs. Yellow fluorescence was displayed in C6@aPDL1-SSLs (pH 7.4) group due to colocalization with the secondary antibody,while the C6@SSL showed no yellow fluorescence,conforming the aPDL1 existed on the surface of liposomes in C6@aPDL1-SSL(pH7.4) group (Figure 3).Moreover, no significant yellow fluorescence was observed from C6@aPDL1-SSLs (pH 6.5), likely owing to the hydrazone bond on the surface of immunoliposomes. The hydrazone bond was cleaved after reacting with H^+ in solution at pH 6.5 and aPDL1 was released (Figure 3). These results suggest that immunoliposomes have pH-sensitive characteristics.

Cellular Uptake of Immunoliposomes in vitro

The cellular uptake of immunoliposomes in vitro was detected by flow cytometry to investigate their specific targeting ability. The coumarin-6(C6), a lipophilic green fluorescent probe, encapsulated liposomes were prepared using the film dispersion method. The results showed no obvious differences in the cellular uptake of C6@SSLs and C6@aPDL1-SSLs at pH 6.5, nor was the uptake of C6@aPDL1-SSLs inhibited after adding free aPDL1 (Figure 4A and C). However, differences were observed at pH 7.4, when the uptake of C6@aPDL1-SSLs was significantly higher than that of C6@SSLs and was inhibited by free aPDL1 (Figure 4B and D). This may be due to cleavage of the pH-sensitive hydrazone bond on the surface of the immunoliposomes at pH 6.5, reacting with H^+ and releasing aPDL1 (Figure 1). These results indicate that the immunoliposomes may consume excessive H^+ in tumor microenvironments, thereby improving inhibitory microenvironments. When aPDL1 was released at pH 6.5, the immunoliposomes were taken up into B16-F10 cells by endocytic pathways

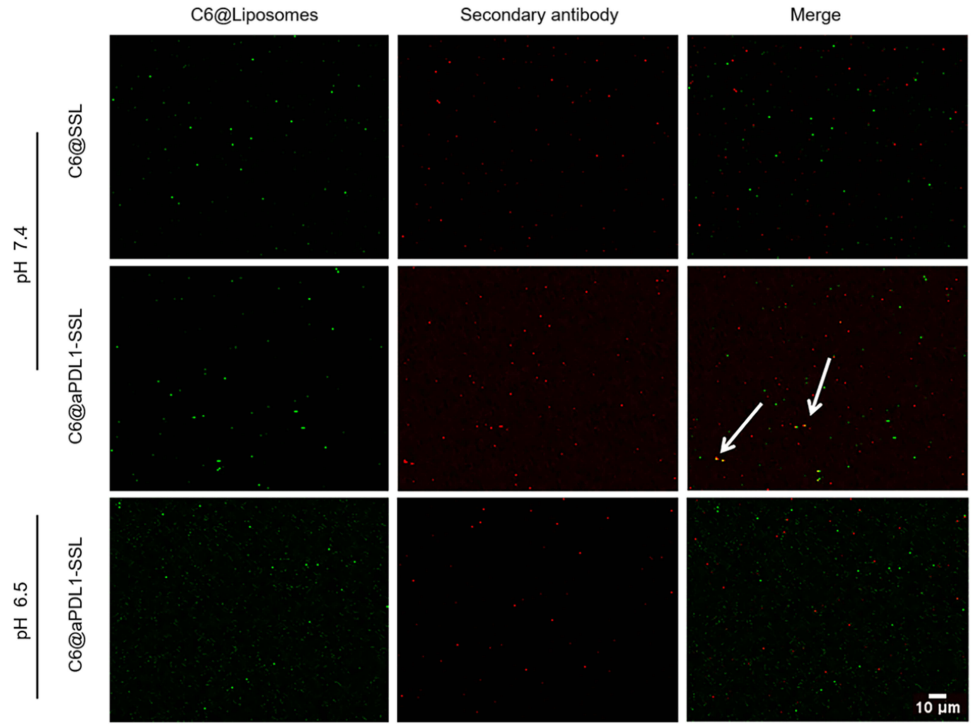

Figure 3 Colocalization results of C6@SSLs, C6@aPDL1-SSLs (pH 7.4), and C6@aPDL1-SSLs (pH 6.5).
Notes: The colocalization results were observed by CLSM. The green signals represented C6@SSLs, C6@aPDL1-SSLs (pH 7.4) or C6@aPDL1-SSLs (pH 6.5) and the red signals represented Alexa Fluor 647-labelled secondary antibodies. The white arrow indicated the colocalization area. Scale bar: 10 μm.
Abbreviations: C6, Coumarin-6; C6@SSLs,C6-loaded liposomes; C6@aPDL1-SSLs, C6-loaded immunoliposomes; CLSM, confocal laser scanning microscopy.

like SSLs, and free aPDL1 did not inhibit the uptake.[32] In addition, the immunoliposomes were taken up into B16-F10 cells at higher levels than SSLs at pH 7.4, and their uptake was inhibited by free aPDL1. This finding suggests that aPDL1 successfully conjugated with the immunoliposomes on the surface, and that immunoliposomes were likely taken up through a receptor-dependent pathway at pH 7.4. Accordingly, because of the overexpression of PD-L1 receptors on B16-F10 cells,[4] immunoliposomes may be promising candidates for melanoma immunotherapy owing to their targeting ability and accumulation in tumor tissue.

Biodistribution of Immunoliposomes in vivo

It was necessary to investigate the biodistribution of immunoliposomes in vivo because biodistribution can influence the therapeutic efficiency and side effects of immunoliposomes. Accordingly, the biodistribution of immunoliposomes was studied using an in vivo optical imaging system. DiR, a lipophilic fluorescent probe, was encapsulated in liposomes. To illustrate the targeting ability of immunoliposomes, free DiR, DiR@SSLs, or DiR@aPDL1-SSLs were intravenously injected into tumor-bearing mice (aPDL1: 1 mg/kg). Following administration, DiR@aPDL1-SSLs gradually accumulated in the tumor tissue. After 24 h, DiR@aPDL1-SSLs emitted the strongest fluorescence signal in the tumor area. This suggests that immunoliposomes had a better tumor-targeting ability than free DiR and DiR@SSLs (Figure 5A).

To further test the targeting ability of immunoliposomes in vivo, tumor-bearing mice were sacrificed 24 h after injection, and their main organs and tumor tissues were harvested for observation (Figure 5B). DiR@aPDL1-SSLs exhibited significant accumulation in tumor tissue, whereas free DiR and DiR@SSLs did not exhibit any obvious accumulation in tumor tissue. Quantitative results showed that the fluorescence efficiency of DiR@aPDL1-SSLs in tumor tissue was the highest among the three treatment groups, 8.5 times higher than the fluorescence efficiency of DiR. DiR@SSLs displayed a lower fluorescence efficiency, 5 times that of free DiR (Figure 5C). Moreover, in vivo distribution showed that the immunoliposomes had the most effective targeting ability compared to free drugs and normal liposomes. This is probably owing to a combination of active targeting and the EPR effect, suggesting that immunoliposomes have the highest

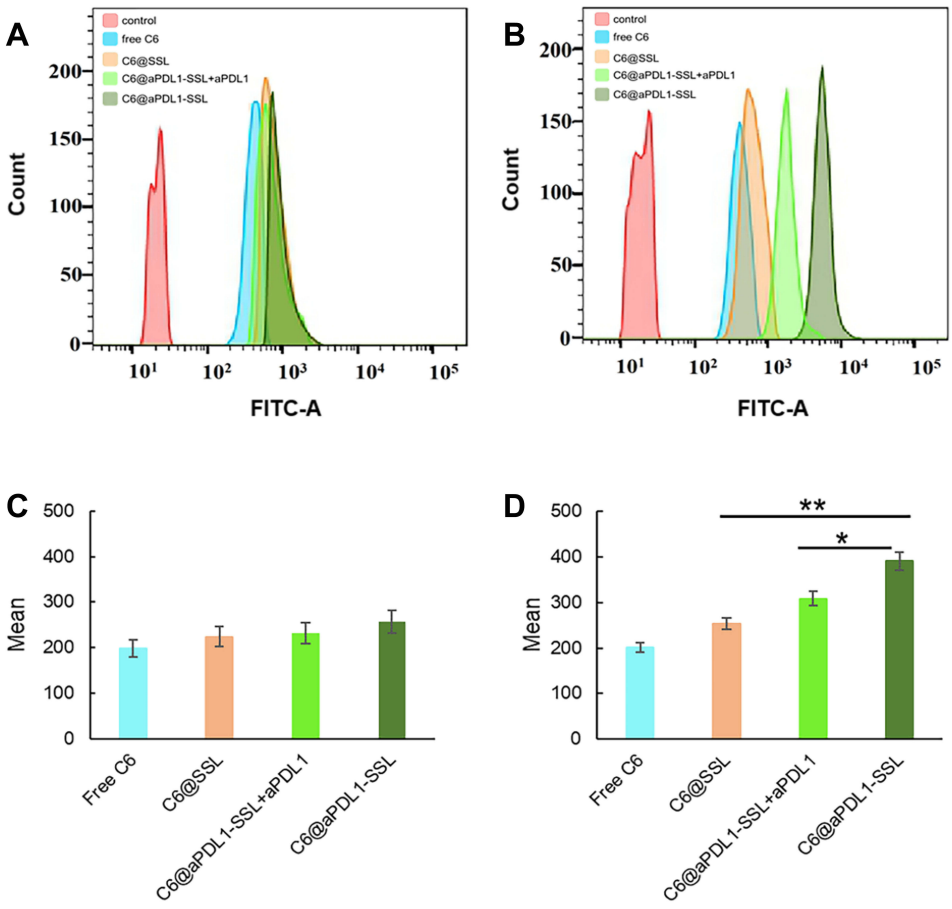

Figure 4 Flow cytometry histograms and mean value of different formulations under different pH conditions.
Notes: (**A, C**) pH 6.5. (**B, D**) pH 7.4. (n = 3, results are shown as means ± S.D. *P < 0.05, **P < 0.01.).
Abbreviations: C6, Coumarin-6; C6@SSLs,C6-loaded liposomes; C6@aPDL1-SSLs, C6-loaded immunoliposomes.

immunotherapeutic efficiency and cause the least side effects in vivo. It is also noteworthy that free DiR showed lower distributions in the liver and spleen compared to liposomes, likely owing to the faster metabolism of free small molecules and the long circulation of liposomes owing to the action of the PEG hydration layer on the surface.[33,34] These findings further support that immunoliposomes are promising candidates for effective immunotherapy in vivo.

Effect of Immunoliposomes on Tumor Hypoxia Status

To demonstrate the effect of immunoliposomes on tumor hypoxia status, we observed the tumor hypoxia area following administration using the immunofluorescence staining method with pimonidazole as exogenous hypoxia-staining probe[31] and hypoxia induced factor (HIF)-1α as the endogenous hypoxia repoter.[17] B16-F10 tumor-bearing mice were randomly divided into four groups and intravenously injected with PBS, aPDL1-SSLs, CAT@SSLs, or CAT@aPDL1-SSLs (CAT: 2 mg/kg, aPDL1: 1 mg/kg). At 24 h following administration, the mice in each group were intraperitoneally injected with pimonidazole (30 mg/kg). The mice were then sacrificed after 90 min to harvest the tumor tissues to observe the tumor hypoxia status via immunofluorescence staining. Hypoxia status was ameliorated following treatment with CAT@SSLs and CAT@aPDL1-SSLs compared to PBS and aPDL1-SSL controls (Figure 6A). In addition, semi-quantitative results showed that after treatment with CAT @ SSL and CAT @ aPDL1-SSL, respectively, the hypoxia positive areas were significantly decreased (Figure 6B). Similarly,the expression levels of HIF-1α protein of tumors collected from mice 24h after injection of CAT @ SSL and CAT @ aPDL1-SSL also showed significant decrease (Figure S3A and B). These results suggest that the CAT-encapsulating liposomes effectively relieved tumor hypoxia through the activity of CAT, which decomposes endogenous H_2O_2 into O_2.[17,18] Hypoxia is an important component of the

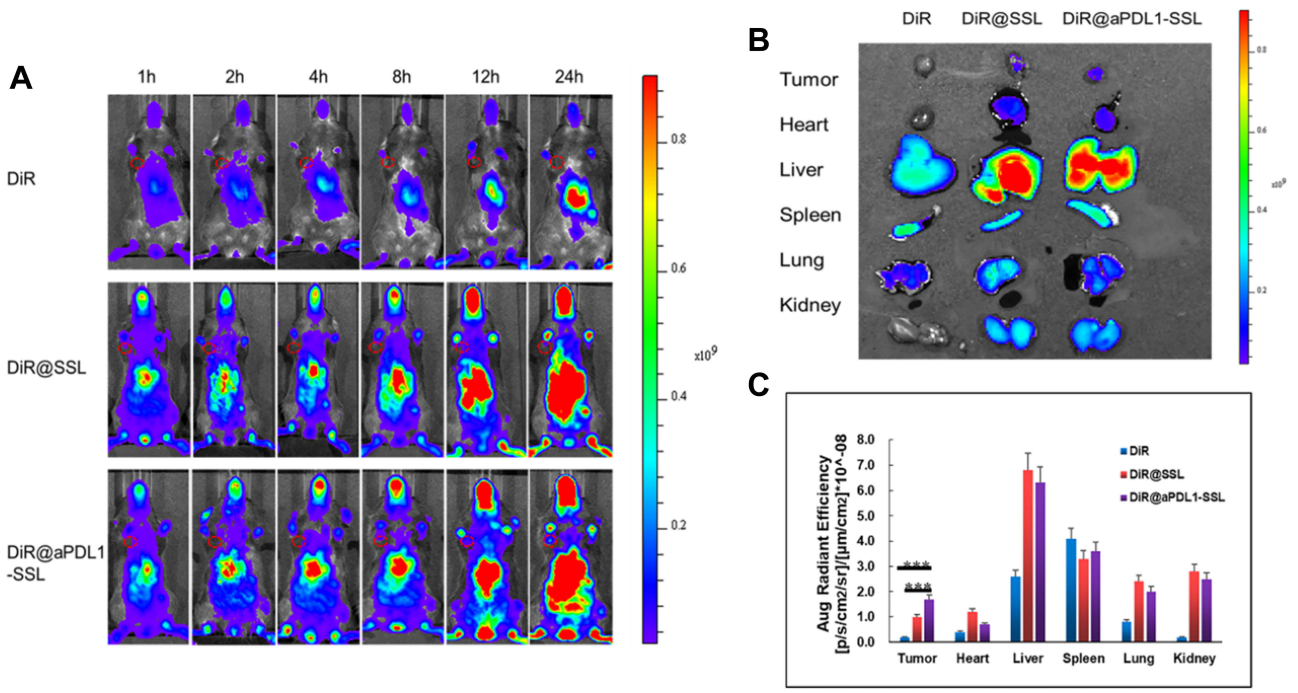

Figure 5 Biodistribution of free DiR, DiR@SSLs, and DiR@aPDL1-SSLs.

Notes: (**A**) In vivo fluorescence images of B16-F10 tumor-bearing mice after intravenous injection of the three formulations at 1, 2, 4, 8, 12, and 24 h (red circle represents the tumor area). (**B**) Ex vivo fluorescence images and (**C**) quantitative results of fluorescence efficiency of main organs and tumor tissues of the three groups 24 h after injection. (n = 3, results are shown as means ± S.D. ***P < 0.001.)

Abbreviations: DiR, 1,1-dioctadecyl-3,3,3,3-tetramethylindotricarbocyanine; DiR@SSLs, DiR-loaded liposomes; DiR@aPDL1-SSLs,DiR- loaded immunoliposomes.

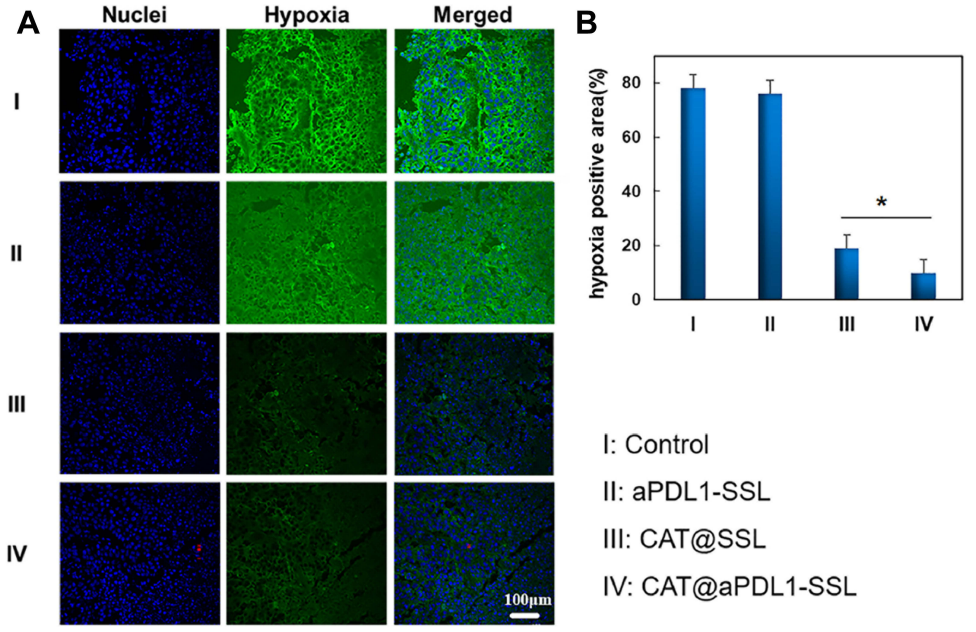

Figure 6 Effects of control (PBS), aPDL1-SSLs, CAT@SSLs, and CAT@aPDL1-SSLs on tumor hypoxia status.

Notes: (**A**) Immunofluorescence images of tumor slices harvested from B16-F10 tumor-bearing mice following intravenous injection with four different formulations. The blue signals represent nuclei stained by DAPI and the green signals represent hypoxia areas stained by hypoxia probe, respectively. (**B**) The quantitative results of positive tumor hypoxia areas analyzed using Image J software based on the images shown in (**A**). (n = 3, results are means ± S.D., Scale bar: 100 μm,*P < 0.05)

Abbreviations: aPDL1, programmed death ligand 1 monoclonal antibody; CAT, catalase; SSL, sterically stabilized liposome; aPDL1-SSLs, aPDL1 modified immunoliposomes; CAT@aPDL1-SSLs, CAT-loaded immunoliposomes.

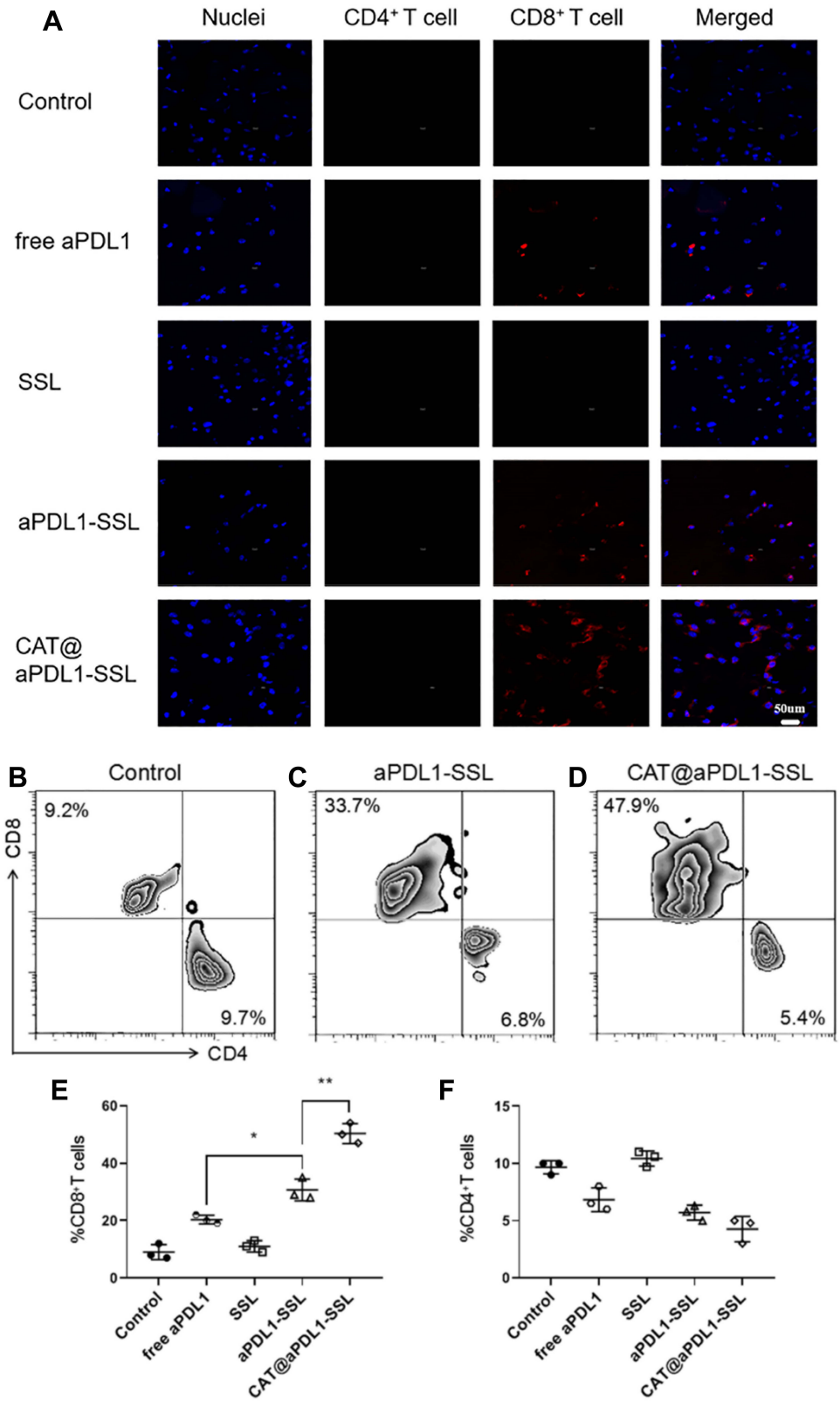

Figure 7 Immunofluorescence of tumor slices and flow cytometry analysis showing $CD4^+$ and $CD8^+$ T cell infiltration.

Notes: (**A**) Immunofluorescence of tumor slices.The blue signals represent nuclei stained with DAPI. The green signals represent $CD4^+$ T cells stained with AF488-$CD4^+$ antibodies and the red signals represent $CD8^+$ T cells stained with AF647-$CD8^+$ antibodies. (Scale bar: 50 μm). (**B, C** and **D**) Flow cytometry analysis and (**E** and **F**) their corresponding percentage of $CD8^+$ and $CD4^+$ tumor infiltrating T cells (n = 3, results are means ± S.D.,*P < 0.05,**P < 0.01).

Abbreviations: aPDL1, programmed death ligand 1 monoclonal antibody; CAT, catalase; SSL, sterically stabilized liposome; aPDL1-SSLs, aPDL1 modified immunoliposomes; CAT@aPDL1-SSLs, CAT-loaded immunoliposomes.

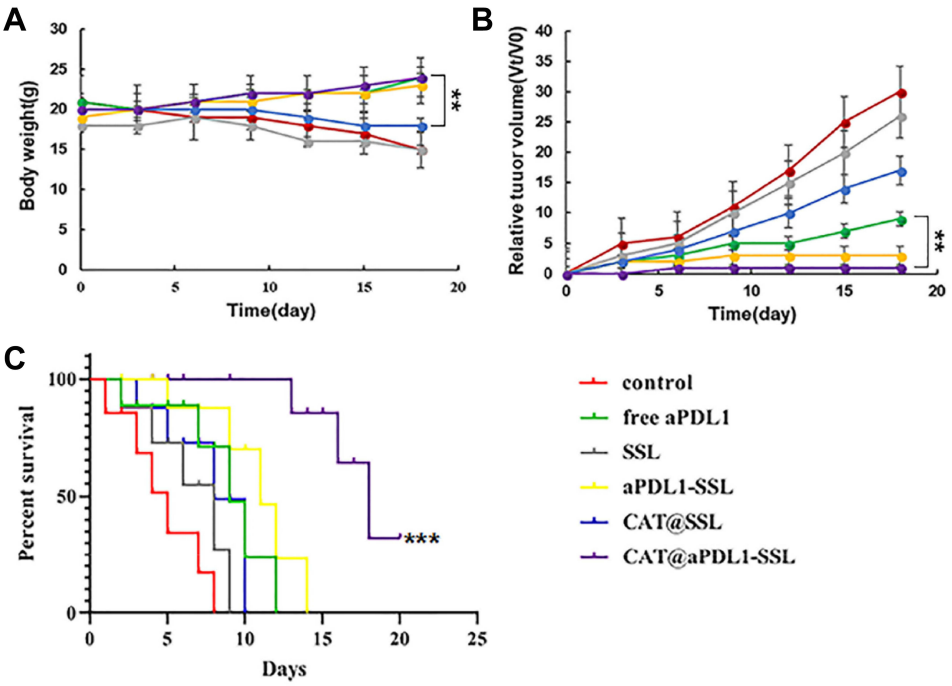

Figure 8 Antitumor efficacy in vivo.
Notes: (**A**) The body weights of B16-F10 tumor-bearing mice after injection with PBS, free aPDL1, SSLs, aPDL1-SSLs, CAT@SSLs, and CAT@aPDL1-SSLs. (**B**) The relative tumor volume of mice in each group. (**C**) Survival curves of mice after treatment with the formulations described above. (n = 6, results means ± S.D., **P < 0.01, ***P < 0.001)
Abbreviations: aPDL1, programmed death ligand 1 monoclonal antibody; CAT, catalase; SSL, sterically stabilized liposome; aPDL1-SSLs, aPDL1 modified immunoliposomes; CAT@aPDL1-SSLs, CAT-loaded immunoliposomes.

tumor-suppressive microenvironment and has a negative regulatory effect on the activation of T cells.[13] Herein, it was reasonable to believe that liposomes encapsulated CAT may display enhanced immunotherapeutic efficiency by relieving hypoxia effectively. Further,CAT@aPDL1-SSLs relieved hypoxia more effectively than CAT@SSLs, likely owing to the targeting distribution and selective accumulation of CAT@aPDL1-SSLs in tumor tissue. These results further suggest that the combination of aPDL1s and CAT is a promising candidate for melanoma immunotherapy in vivo.

T-Cell-Mediated Immune Responses

The infiltration of T lymphocytes in tumor tissues was investigated because it is an important indicator for evaluating the therapeutic effects of immunoliposomes. The infiltration of $CD4^+$ and $CD8^+$ T cells in tumor tissues was observed after treatment with PBS, free aPDL1, SSLs, aPDL1-SSLs, or CAT@aPDL1-SSLs (CAT: 2 mg/kg; aPDL1: 1 mg/kg) using immunofluorescence staining and flow cytometry analysis. The tumor tissues in the control PBS group had little $CD8^+$ T cell infiltration, whereas the tumor tissues in the CAT@aPDL1-SSLs group had significant $CD8^+$ T cell infiltration (Figures 7A–F and S4). In particular, there were more $CD8^+$ T cells infiltrating the tumor tissues in the aPDL1-SSL group than in the free aPDL1 group, suggesting that the therapeutic effects of aPDL1s were improved by conjugation on the surface of liposomes due to the EPR effect and active targeting. Moreover, the tumor tissues in the CAT@aPDL1-SSL-treated group were infiltrated with higher levels of $CD8^+$ T cells than those in the aPDL1-SSL group. This suggests that CAT@aPDL1-SSLs may effectively promote the infiltration of $CD8^+$ T cells in tumor tissues, likely owing to the synergistic therapeutic effects of aPDL1s and CAT. These findings also suggest that the immunotherapeutic effects of CAT@aPDL1-SSLs were mainly associated with $CD8^+$ T cells.

Antitumor Efficacy and Safety in vivo

To demonstrate the immunotherapeutic efficiency of the immunoliposomes in vivo, control (PBS), free aPDL1, SSLs, aPDL1-SSLs, CAT@SSLs, or CAT@aPDL1-SSLs were intravenously injected into B16-F10 tumor-bearing mice every 3 days. The weights of the mice and tumor volumes were measured every 3 days. CAT@aPDL1-SSLs exhibited a superior therapeutic effect (Figure 8A–C).

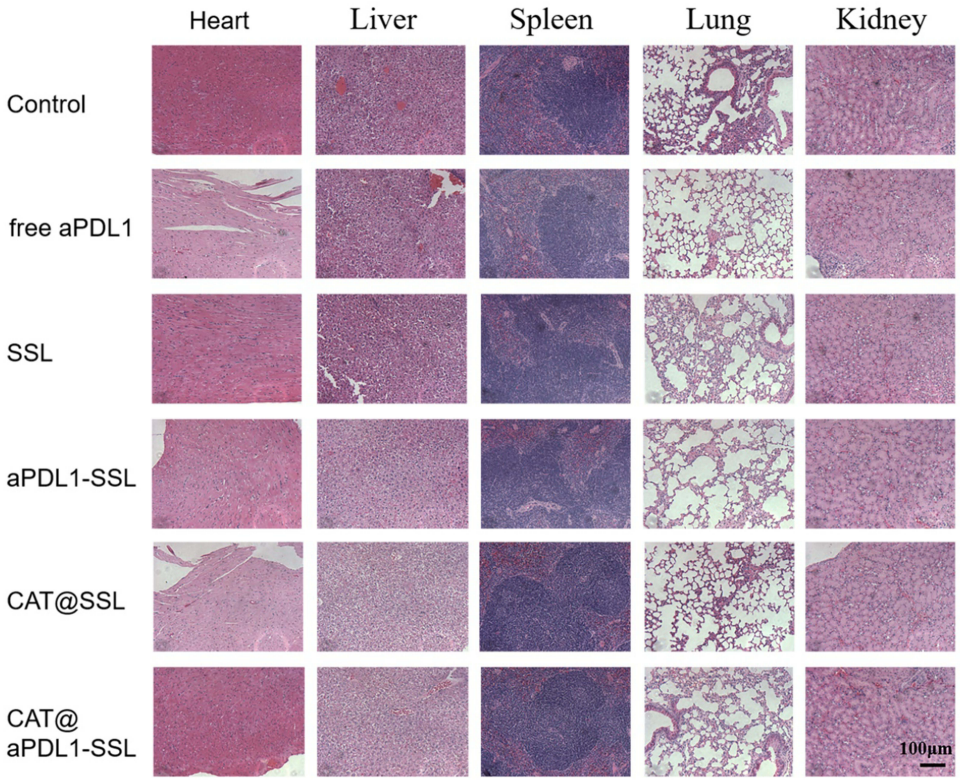

Figure 9 Safety assessment of different formulations in vivo.
Notes: The morphology of the main organs, including the heart, liver, spleen, lungs, and kidneys were observed using the H&E staining method after treating mice with PBS, free aPDL1, SSLs, aPDL1-SSLs, CAT@SSLs, or CAT@aPDL1-SSLs (Scale bar: 100 μm).
Abbreviations: aPDL1, programmed death ligand 1 monoclonal antibody; CAT, catalase; SSL, sterically stabilized liposome; aPDL1-SSLs, aPDL1 modified immunoliposomes; CAT@aPDL1-SSLs, CAT-loaded immunoliposomes.

The weights of mice in the aPDL1, aPDL1-SSL, and CAT@aPDL1-SSL groups increased slightly, whereas the weights of mice in the other groups decreased (Figure 8A), possibly owing to the systemic symptoms caused by tumors. The tumor volume in the CAT@aPDL1-SSL group remained largely unchanged. However, tumor volumes increased by nearly 9.25-fold and 3.69-fold in the free aPDL1 and aPDL1-SSL treatment groups, respectively, compared to the primary (Figure 8B). These results suggest that liposomes, as nanocarriers, enhanced the treatment effects of aPDL1, likely due to the EPR effect and active targeting. The combination of aPDL1 and CAT appeared to be an effective strategy for producing synergistic therapeutic effects. Only mice in the CAT@aPDL1-SSL group survived until the end of the experiment (Figure 8C), further supporting that CAT@aPDL1-SSLs had anti-tumor efficacy consistent with other results of this study.

The in vivo safety of immunoliposomes was investigated via H&E staining. The morphology of the main organs, including the heart, liver, spleen, lungs, and kidneys, showed no obvious pathological abnormalities after treatment with different formulations (Figure 9). CAT@aPDL1-SSLs appeared to be safe, and did not produce systemic toxicity after continuous administration. Accordingly, these results suggest that the immunoliposomes developed in this study may not only have superior anti-tumor efficacy, but also great safety, making them promising candidates for melanoma immunotherapeutic treatment in vivo.

Conclusion

To overcome these limitations and enhance the immunotherapeutic efficiency of aPDL1s, we develop multifunctional immunoliposomes, called CAT@aPDL1-SSLs, modified with aPDL1 on the surface and CAT encapsulated inside. The efficacy of CAT@aPDL1-SSLs is verified by multiple experiments in vivo and in vitro. The results of the various experiments in this study suggest that multifunctional immunoliposomes combining CAT and aPDL1 are promising candidates for melanoma immunotherapy for at least three reasons. First, immunoliposomes can be easily prepared and have great targeting ability, accumulating specifically in

tumor tissue, thus reducing systemic toxicity. Second, immunoliposomes combining CAT and aPDL1 produce synergistic effects that enhance immunotherapeutic efficiency by blocking the PD-1/PD-L1 pathway and relieving tumor hypoxia. Third, immunoliposomes inhibited the growth of melanoma and prolonged the survival time of tumor-bearing mice. In conclusion, the multifunctional immunoliposomes developed and proposed in this study are a promising candidate for melanoma immunotherapy, and could potentially be combined with other cancer therapies like radiotherapy and chemotherapy to produce positive outcomes.

Acknowledgments

This work was afforded by the National Natural Science Foundation of China (No. 81571824) and Regenerative Innovation Program of AAIS-HGB, Peking University.

Disclosure

The authors report no conflicts of interest in this work.

References

1. Shergold AL, Millar R, Nibbs RJB. Understanding and overcoming the resistance of cancer to PD-1/PD-L1 blockade. *Pharmacol Res*. 2019;145:104–258. doi:10.1016/j.phrs.2019.104258
2. Minn AL, Wherry EJ. Combination cancer therapies with immune checkpoint blockade: convergence on interferon signaling. *Cell*. 2016;165:272–275. doi:10.1016/j.cell.2016.03.031
3. Gajewski TF, Schreiber H, Fu YX. Innate and adaptive immune cells in the tumor microenvironment. *Nat Immunol*. 2013;14:1014−1022. doi:10.1038/ni.2703
4. Leisegang M, Kammertoens T, Uckert W, et al. Targeting human melanoma neoantigens by T cell receptor gene therapy. *J Clin Invest*. 2016;126:854–858. doi:10.1172/JCI83465
5. Eroglu Z, Zaretsky JM, Hu-lieskovan S, et al. High response rate to PD-1 blockade in desmoplastic melanomas. *Nature*. 2018;553:347–350. doi:10.1038/nature25187
6. Naidoo J, Page DB, Li BT, et al. Toxicities of the anti-PD-1 and anti-PD-L1 immune checkpoint antibodies. *Ann Oncol*. 2015;26:2375–2391. doi:10.1093/annonc/mdv383
7. Mellati M, Eaton KD, Brooks-worrell BM, et al. Anti-PD-1 and anti-PDL-1 monoclonal antibodies causing type 1 diabetes. *Diabetes Care*. 2015;38:137–138. doi:10.2337/dc15-0889
8. Boutros C, Tarhini A, Routier E, et al. Safety profiles of anti-CTLA-4 and anti-PD-1 antibodies alone and in combination. *Nat Rev Clin Oncol*. 2016;13:473–486. doi:10.1038/nrclinonc.2016.58
9. Postow MA. Managing immune checkpoint-blocking antibody side effects. *Am Soc Clin Oncol Educ B*. 2015;35:76–83. doi:10.14694/EdBook_AM.2015.35.76
10. Weber JS, Yang JC, Atkins MB, et al. Toxicities of immunotherapy for the practitioner. *J Clin Oncol*. 2015;33:2092–2099. doi:10.1200/JCO.2014.60.0379
11. Powles T, Eder JP, Fine GD, et al. MPDL3280A (anti-PD-L1) treatment leads to clinical activity in metastatic bladder cancer. *Nature*. 2014;515:558–562. doi:10.1038/nature13904
12. Noman MZ, Hasmim M, Messai Y, et al. Hypoxia: a key player in antitumor immune response. A review in the theme: cellularResponses to hypoxia. *Am J Physiol Cell Physiol*. 2015;309:569–579. doi:10.1152/ajpcell.00207.2015
13. Gajewski TF, Woo SR, Zha Y, et al. Cancer immunotherapy strategies based on overcoming barriers within the tumor microenvironment. *Curr Opin Immunol*. 2013;25:268–276. doi:10.1016/j.coi.2013.02.009
14. Shi S, Chen L, Huang G. Antiangiogenic therapy improves the antitumor effect of adoptive cell immunotherapy by normalizing tumor vasculature. *Med Oncol*. 2013;30:1–7. doi:10.1007/s12032-013-0698-1
15. Tao JH, Barbi J, Pan F. Hypoxia-inducible factors in T lymphocyte differentiation and function. A review in the theme: cellular responses to hypoxia. *Am J Physiol Cell Physiol*. 2015;309:580–589. doi:10.1152/ajpcell.00204.2015
16. Zhang Y, Ertl HC. Starved and asphyxiated: how can CD8(+) T cells within a tumor microenvironment prevent tumor progression. *Front Immunol*. 2016;32:1–7.
17. Chouaib S, Noman MZ, Kosmatopoulos K, et al. Hypoxic stress: obstacles and opportunities for innovative immunotherapy of cancer. *Oncogene*. 2017;36:439–445. doi:10.1038/onc.2016.225
18. Song G, Liang C, Gong H, et al. Core-shell MnSe@Bi2 Se3 fabricated via a cation exchange method as novel nanotheranostics for multimodal imaging and synergistic thermoradiotherapy. *Adv Mater*. 2015;27:6110–6117. doi:10.1002/adma.201503006
19. Felice B, Prabhakaran MP, Rodríguez AP, et al. Drug delivery vehicles on a nano-engineering perspective. *Mater Sci Eng C Mater Biol Appl*. 2015;41:178–195. doi:10.1016/j.msec.2014.04.049
20. Fanciullino R, Ciccolini J. Liposome-encapsulated anticancer drugs: still waiting for the magic bullet? *Curr Med Chem*. 2009;16:4361–4373. doi:10.2174/092986709789712916
21. Allen TM, Cullis PR. Liposomal drug delivery systems: from concept to clinical applications. *Adv Drug Deliv Rev*. 2013;65:36–48. doi:10.1016/j.addr.2012.09.037
22. Shao K, Singha S, Clemente-casares X, et al. Nanoparticle-based immunotherapy for cancer. *ACS Nano*. 2015;9:16–30. doi:10.1021/nn5062029
23. Zili G, Wang Q, Shi Y, et al. Nanotechnology-mediated immunochemotherapy combined with docetaxel and PD-L1 antibody increase therapeutic effects and decrease systemic toxicity. *J Control Release*. 2018;286:369–380. doi:10.1016/j.jconrel.2018.08.011
24. Hongwei Z. Thin-film hydration followed by extrusion method for liposome preparation. *Methods Mol Biol*. 2017;1522:17–22.
25. Arabi L, Badiee A, Mosaffa F, et al. Targeting CD44 expressing cancer cells with anti-CD44 monoclonal antibody improves cellular uptake and antitumor efficacy of liposomal doxorubicin. *J Control Release*. 2015;220:275–286. doi:10.1016/j.jconrel.2015.10.044
26. Xu S, Cui F, Huang D, et al. PD-L1 monoclonal antibody-conjugated nanoparticles enhance drug delivery level and chemotherapy efficacy in gastric cancer cells. *Int J Nanomedicine*. 2019;14:17–31. doi:10.2147/IJN.S175340
27. Song G, Chen Y, Liang C, et al. Catalase-loaded TaOx nanoshells as bio-nanoreactors combining high-Z element and enzyme delivery for enhancing radiotherapy. *Adv Mater*. 2016;28:7143–7148. doi:10.1002/adma.201602111
28. Goth L. A simple method for determination of serum catalase activity and revision of reference range. *Clin Chim Acta*. 1991;196:143–151. doi:10.1016/0009-8981(91)90067-M
29. Kobayashi H, Watanabe R, Choyke PL. Improving conventional enhanced permeability and retention (EPR) effects; what is the appropriate target? *Theranostics*. 2014;4:81–89. doi:10.7150/thno.7193
30. Southan C, Williams AJ, Ekins S. Challenges and recommendations for obtaining chemical structures of industry-provided repurposing candidates. *Drug Discov Today*. 2013;18:58–70. doi:10.1016/j.drudis.2012.11.005
31. Zhang R, Song X, Liang C, et al. Catalase-loaded cisplatin-prodrug-constructed liposomes to overcome tumor hypoxia for enhanced chemo-radiotherapy of cancer. *Biomaterials*. 2017;138:13–21. doi:10.1016/j.biomaterials.2017.05.025

32. Zhao BX, Zhao Y, Huang Y, et al. The efficiency of tumor-specific pH-responsive peptide-modified polymeric micelles containing paclitaxel. *Biomaterials*. 2012;33:2508–2520. doi:10.1016/j.biomaterials.2011.11.078
33. Cevc G, Blume G. Hydrocortisone and dexamethasone in very deformable drug carriers have increased biological potency, prolonged effect, and reduced therapeutic dosage. *BBA-Biomembranes*. 2004;1663:91–97. doi:10.1016/j.bbamem.2004.01.006
34. Klibanov AL, Maruyama K, Beckerleg AM, et al. Activity of amphipathic poly (ethylene glycol) 5000 to prolong the circulation time of liposomes depends on the liposome size and is unfavorable for immunoliposome binding to target. *Biochim Biophys Acta*. 1991;1062:142–148. doi:10.1016/0005-2736(91)90385-L